

Impulse-response analysis of planar computed tomography for nondestructive test

Daechon Kim^a, Seung Ho Kim^a, Ho Kyung Kim^{a,b*}

^aSchool of Mechanical Engineering, Pusan National University, Busan, South Korea

^bCenter for Advanced Medical Engineering Research, Pusan National University, Busan, South Korea

*Corresponding author: hokyung@pusan.ac.kr

1. Introduction

There have been reported that the use of radiation imaging such as digital radiography, computed tomography (CT), and digital tomosynthesis (DTS) for the nondestructive test (NDT) widely is spreading. These methods have merits and demerits of their own, in terms of image quality and inspection speed. Therefore, they are separately used to compatible aim of applications. For the industrial applications, such as multi-layer printed circuit board (PCB) inspection, the automated inspection systems should be conducted for real time imaging. Therefore, image for these methods for NDT should have acceptable image quality and high speed.

In this study, we quantitatively evaluate impulse responses of reconstructed images from the filtered backprojection (FBP), which are most widely used in planar computed tomography (pCT) systems. We first evaluate image performance metrics due to the contrast, depth resolution, and then we design the figure of merit including image performance and system parameters, such as tube load and reconstruction speed.

2. Materials and Methods

2.1 Filtered Backprojection

In this study, we chose filtered backprojection for the analytic image reconstruction. The most popular image reconstruction algorithm in DTS is the Feldkamp (FDK) type algorithm. The main characteristics of the algorithm is parallel beam approximation during the backprojection procedure of con beam geometry. The FDK can be represented by following equation [1].

$$f(r) = \int_{\phi_{\min}}^{\phi_{\max}} d\phi \frac{L^2}{(\lambda - r \cdot (\mathbf{n}_\zeta \times \mathbf{n}_\eta))^2} [\tilde{p}_\phi(\zeta, \eta) * \mathbf{h}(\zeta)], \quad (1)$$

where L is the distance from source to detector, λ is the distance from source to rotation center, and $f(r)$ is an object function in spatial coordinate. $\tilde{p}_\phi(\zeta, \eta)$ represents projection image multiplied by distance weighting.

The weighting function in equation (1) makes approximately cone beam to parallel beam geometry. $h(\zeta)$ in equation (1) represents filtering operation, we use hanning window as usual filter for cone beam computed tomography (CBCT) and additional slice

thickness filter for DTS is applied to compensate data deficit because of limited scan angle [5].

2.2 Comparison metric

The important image performances of the DTS systems are contrast and depth resolution. To compare these characteristics between the FBP and the SART, we used the quantitative metrics such as signal difference-to-noise ratio (SDNR) and artificial-spread function (ASF). The SDNR characterizes the contrast in the slice images. The SDNR is represented by the following equation:

$$\text{SDNR} = \frac{S_R - S_B}{\sigma_B}, \quad (8)$$

where S_R is signal in the lesion, S_B is signal in the background, and σ_B is noise in the background.

Another important consideration of DTS system is the depth resolution, which is degraded by depth-directional blur artifact caused by the limited angular range of the system. The ASF, which evaluates the depth resolution of DTS systems, was first introduced by Wu *et al* [4]. It is defined by the ratio of pixel intensity between focal plane and the other planes. Therefore, we can have the ASF as [4].

$$\text{ASF} = \frac{S_R(z) - S_B(z)}{S_R(z_0) - S_B(z_0)} \quad (9)$$

where z_0 and z denote the depth of focal plane and the other plane, respectively. Unfortunately, the ASF gives the trend of the blur artifact. Instead, we use half-width at half-maximum (HWHM) of the ASF as a single-valued metric [5].

2.5 Quantitative phantom

We build the lab-made quantitative phantom to measure the SDNR and ASF simultaneously as shown in fig. 1. The phantom contains 1-mm-thick aluminum disk inside the 30-mm-diameter PMMA cylinder. At the center slice, we can calculate low contrast SDNR at the aluminum region and PMMA region. And the ASF can

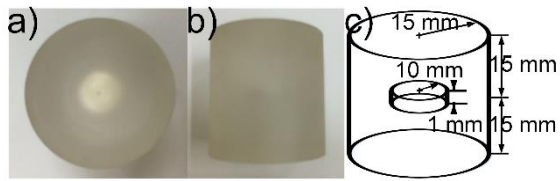


Figure 1. Cylinder phantom to evaluate SDNR, and ASF. (a) A photograph of the cylinder phantom. (b) Dimensions of the phantom.

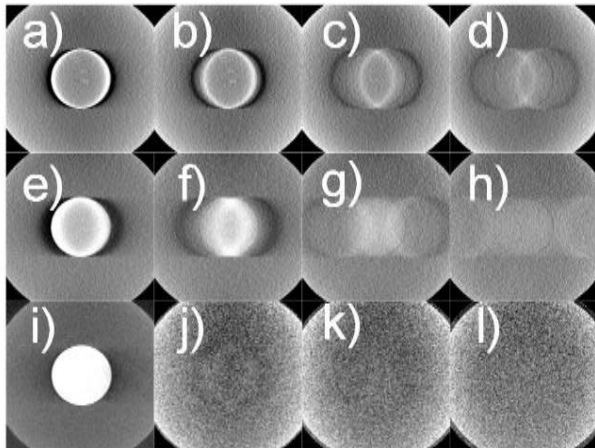


Figure 2. Reconstruction images. (a) - (d), (e) - (h), and (i) - (l) were reconstructed by angular range 60° , 120° , 360° . The first column images are reconstructed images of center, the second ones are 2.5 mm from the center, third ones are 5 mm from the center, and the fourth ones are 7.5 mm from the center

be also calculated by the same regions at the different depth position.

3. PRELIMINARY RESULT

Figure 2 shows the reconstructed slice images of quantitative phantom depicted in fig. 2 by the FBP algorithm. The projection images are taken from angular range of 60° , 120° , and 360° . The slices are selected at the focal plane (a), and 2.5 mm (b), 5 mm, and 7.5 mm apart from the focal plane, respectively. The (e) - (h), and (i) - (l) show the slice images taken from the angular range of 120° , and 360° . All the imaging parameters except angular range were determined along with 60° case.

Figure 3 and 4 show the results of SDNR and ASF from the reconstructed images. The result of SDNR increases when the angular range is increasing from the fig. 3. It also depends on the number of views when the condition of angular range is same.

The ASF also improves in the condition of wider angular range from fig. 4.

4. FURTHER STUDY

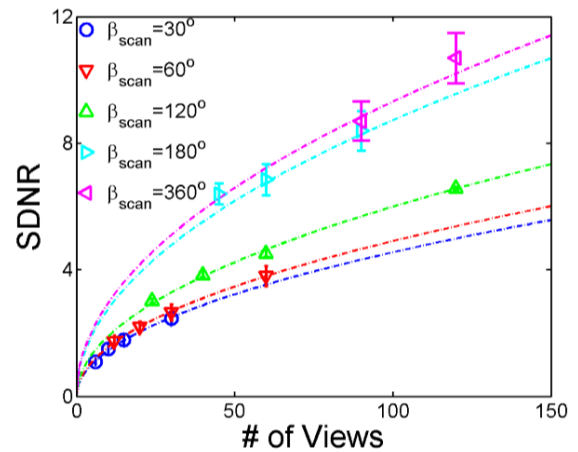


Figure 3. It represents SDNR of the central slice results from various angular range. It is mainly depends on the angular range, and the number of views is affected when the angular range is same.

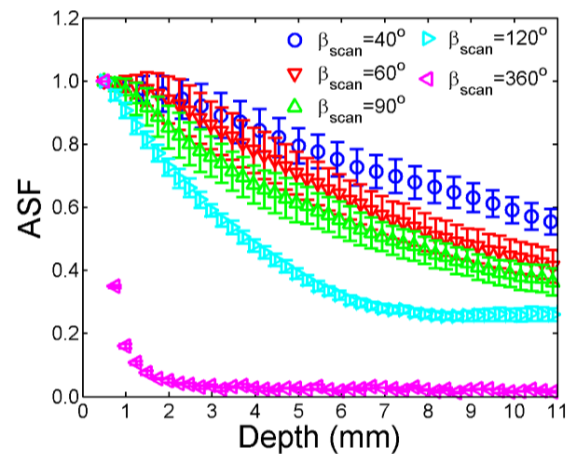


Figure 4. It shows the result of ASF from various angular range and step angle is 1° . It shows the depth resolution of the reconstruction images are mainly depends on the angular range

The final goal of this study is the application of these methods to the nondestructive test. In order to accomplish it, further study is needed. First of all, the results of the ASF from various numbers of views. Second, the analysis of modulation transfer function, noise power spectrum, and detective quantum efficiency from various angular range and numbers of views. And finally, it should be verified by experiment that the algorithm works correctly. Once we prove the algorithm is correct for the PCB phantom, then the results of reconstruction images will be compared by using metric parameters.

ACKNOWLEDGEMENT

This work was supported by the National Research Foundation of Korea (NRF) grant funded by the Korea government (MSIP) (No. 2013M2A2A9046313).

REFERENCES

- [1] L. A. Feldkamp, L. C. Davis, and J. W. Kress, Practical cone-beam algorithm, *J. Opt. Soc. Am. A.*, Vol. 1, pp. 612-619, 1984.
- [2] A. C. Kak and M. Slaney, Principles of computerized tomographic imaging, IEEE press, New York, 1988.
- [3] G. Lauritsch and W. H. Härer, Theoretical framework for filtered back projection in tomosynthesis, *Proc. SPIE*, Vol. 3338, pp. 1127–1137, 1998.
- [4] T. Wu, R. H. Moore, E. A. Rafferty, and D. B. Kopans, A comparison of reconstruction algorithms for breast tomosynthesis, *Med. phys.*, Vol. 31, pp. 2636–2647, 2004.
- [5] H. Youn, J. S. Kim, M. K. Cho, S. Y. Jang, W. Y. Song, and H. K. Kim, Optimizing imaging conditions in digital tomosynthesis for image-guided radiation therapy, *Korean J. Med. Phys.*, Vol. 21, pp. 281-290, 2010.